Mismatched Finite-Complexity MMSE Decision Feedback Equalizers

Naofal Al-Dhahir *, Member, IEEE, and John M. Cioffi, Fellow, IEEE

Abstract

Closed–form expressions that quantify the degradation in the decision–point signal–to–noise ratio of the finite–length minimum mean–square–error decision feedback equalizer (MMSE—DFE) due to channel and noise mismatch conditions are derived. The analysis is further extended to other receiver structures, namely the MMSE–DFE with an adaptive feedforward filter, the MMSE linear equalizer, and the discrete multitone transceiver, *all under a finite–complexity* constraint. The limiting case of infinite–length filters is also analyzed.

In addition, we present computer simulation results that compare the performance of the various receiver structures under study, assuming a particular channel and noise mismatch model for the high–bit–rate digital subscriber loop environment. Finally, several methods that can be used to mitigate the effects of mismatch are outlined.

I. Introduction

Approaching theoretical performance limits on dispersive noisy channels requires optimization of both the transmitter and receiver ends of a communication system. This optimization process is based on accurate knowledge about the channel and noise characteristics. For instance, the optimum feedforward and feedback filter settings of the minimum mean–square–error decision feedback equalizer (MMSE–DFE) are a function of the channel impulse response (CIR) coefficients and the noise auto–correlation sequence [11, 4]. Likewise, channel and noise information is crucial in determining the optimal symbol rate of the input signal (or equivalently the transmission bandwidth) to be used at the transmitter [11, 2]. In practice, the channel and noise characteristics are typically learned by transmitting a training sequence either at the beginning or in the middle of data packets as in the digital cellular standards IS–54 and GSM, respectively.

*This work was supported by NSF under Contract NCR-9203131, JSEP under Contract DAAL 03-91-C-0010, and NASA under Contract NAG2-842. This paper was presented in part at CISS'94.

Unfortunately, a variety of factors can result in a "mismatch" between the channel and noise characteristics assumed in the design of the transmitter and receiver ends and the actual characteristics. We enumerate some of these factors next. First, the inevitable estimation errors associated with channel and noise identification during the training stage, especially when the input SNR is low. Secondly, time variations in the channel and noise characteristics that are much faster than the adaptation speed of the transmitter or receiver (as in some wireless environments). Thirdly, in some applications such as high–speed asymmetric data transmission on digital subscriber loops (ADSL), practical complexity considerations oblige the engineer to assume that the transmission bandwidth of the MMSE–DFE is *fixed at some compromise value* (or at best belongs to a finite pre–determined set of values). The varying channel characteristics across the loop population result in an appreciable performance loss on some loops due to the mismatch between the usable bandwidth and the optimal bandwidth that should be used. Fourthly, as described in [6], significant savings in implementation cost can be achieved in some applications if the MMSE–DFE's long finite–impulse–response (FIR) filters are implemented as pole–zero filters with much fewer coefficients. Inevitable pole–zero modeling errors, albeit being small, contribute to the mismatch. Finally, another source of mismatch can be attributed to finite–precision effects such as quantization and round–off errors. Whatever the cause of the mismatch is, analyzing its effects on performance is of significant importance.

This problem has been previously studied by Gozzo [10] and Tu [14]. In [10], the assumptions of binary signaling, white noise, and infinite–length filters were made. In our analysis, we relax all of these assumptions by considering M-ary signaling, finite–length filters, and colored noise. In addition, we consider other widely–used receiver structures that were not analyzed in [10], namely the adaptive minimum mean–square–error decision feedback equalizer (AMMSE–DFE) and the discrete multitone transceiver (DMT). Our approach is similar to that of [14], except that we treat the more general case of finite–length filters. It is also worth emphasizing that our development differs from that of [10, 14] in that we consider various forms of mismatch including delay mismatch and mismatch due to pole–zero modeling.

The rest of this paper is organized as follows. We shall start in Section II by deriving closed–form expressions that quantify the degradation in the decision-point SNR of the finite-length MMSE–DFE, AMMSE–DFE, and MMSE linear equalizer (LE) due to channel and noise mismatch. These expressions are evaluated for the high–bit–rate digital subscriber loop (HDSL) environment using computer simulations in Section III. This allows us to compare the performance of the three receiver structures under study and investigate the effect of several simulation parameters such as input power, mismatch level, and the number of equalizer taps. Finally, Section IV examines a number of related issues including sensitivity of the DMT to mismatch, means for improving the robustness towards channel and noise mismatch, and the specialization of our results to those of [14, 10] by allowing the equalizer's length to become infinite.

II. Mismatched Receivers

II-A. The Mismatched FIR MMSE-DFE

We shall start with the following discrete–time representation of a linear time–invariant additive–noise FIR channel

$$y_k = \sum_{m=0}^{\nu} h_m x_{k-m} + n_k \ , \tag{1}$$

where ν is called the channel memory. Over a block of N_f output symbols $\mathbf{y}_{k+N_f-1:k}$, Equation (1) can be expressed as follows

$$\mathbf{y}_{k+N_f-1:k} = \mathbf{H}\mathbf{x}_{k+N_f-1:k-\nu} + \mathbf{n}_{k+N_f-1:k} \ ,$$

where $\mathbf{H}$ is an $N_f \times (N_f+\nu)$ Toeplitz channel matrix whose first row is $\begin{bmatrix} h_0 & h_1 & \cdots & h_\nu & 0 & \cdots & 0 \end{bmatrix}$. The input symbols $\mathbf{x}_{k+N_f-1:k-\nu}$ are assumed to be complex, zero–mean, and uncorrelated with an average energy of S_x, i.e., $\mathbf{R}_{xx} \stackrel{def}{=} \mathrm{E}[\mathbf{x}_{k+N_f-1:k-\nu}\mathbf{x}^*_{k+N_f-1:k-\nu}] = S_x \mathbf{I}_{N_f+\nu}$ (where $(.)^*$ denotes the complex–conjugate transpose). The noise symbols $\mathbf{n}_{k+N_f-1:k}$ are assumed to be *independent* of the input symbols $\mathbf{x}_{k+N_f-1:k-\nu}$ and the noise auto–correlation matrix is denoted by $\mathbf{R}_{nn} \stackrel{def}{=} \mathrm{E}[\mathbf{n}_{k+N_f-1:k}\mathbf{n}^*_{k+N_f-1:k}]$. Therefore, the input–output cross–correlation and the output auto–correlation matrices are

$$\begin{aligned} \mathbf{R}_{xy} &\stackrel{def}{=} \mathrm{E}[\mathbf{x}_{k+N_f-1:k-\nu}\mathbf{y}^*_{k+N_f-1:k}] = S_x \mathbf{H}^* \\ \mathbf{R}_{yy} &\stackrel{def}{=} \mathrm{E}[\mathbf{y}_{k+N_f-1:k}\mathbf{y}^*_{k+N_f-1:k}] = S_x \mathbf{H}\mathbf{H}^* + \mathbf{R}_{nn} \ . \end{aligned}$$

We shall denote the misestimated channel matrix and the misestimated noise auto–correlation matrix by $\mathbf{H}^e$ and $\mathbf{R}^e_{nn}$, respectively. The available input power, P, is assumed to be *evenly–distributed over an optimized bandwidth* $W^{opt.}$, i.e., $S_x = \frac{P}{W^{opt.}}$. This optimal bandwidth is a function of the channel and noise characteristics [2]. Therefore, channel and noise estimation errors (CNEE) result in a non–optimum transmission bandwidth, call it W^e, which in turn modifies the input correlation matrix to $\mathbf{R}^e_{xx} = \frac{P}{W^e}\mathbf{I}_{N_f+\nu^e} \stackrel{def}{=} S^e_x \mathbf{I}_{N_f+\nu^e}$ (where ν^e is the misestimated channel memory).

The FIR MMSE–DFE receiver structure consists of two filters : a feedforward filter $\mathbf{w}^*$ that has N_f taps and a strictly–causal feedback filter that is determined by the monic filter $\mathbf{b}$. In this paper, $\mathbf{b}$ *is assumed to have the same number of taps,* $\nu+1$, *as the channel impulse response.*[1] The general case of an FIR MMSE–DFE with a feedback filter that has an arbitrary length is treated in [5].

[1] This assumption simplifies the analysis significantly and offers further insight into the operation of the finite–length MMSE–DFE, as it was demonstrated in detail in [4].

It was shown in [4, 3] that in the absence of CNEE and *assuming correct past decisions*, the optimal feedforward and feedback filter settings that minimize the mean square of the error sequence

$$\begin{aligned} e_k &\stackrel{def}{=} \hat{x}_k - z_k \\ &= \tilde{\mathbf{b}}^* \mathbf{x}_{k+N_f-1:k-\nu} - \mathbf{w}^* \mathbf{y}_{k+N_f-1:k} \ , \end{aligned} \tag{2}$$

are computed from the Cholesky factorization

$$\mathbf{R} \stackrel{def}{=} \frac{1}{S_x}\mathbf{I}_{N_f+\nu} + \mathbf{H}^*\mathbf{R}_{nn}^{-1}\mathbf{H} \stackrel{def}{=} \mathbf{LDL}^* \ , \tag{3}$$

as follows [2]

$$\tilde{\mathbf{b}}_{opt.} \stackrel{def}{=} \begin{bmatrix} \mathbf{0}_{1\times(N_f-1)} & \mathbf{b} \end{bmatrix}^t = \mathbf{L}\mathbf{e}_{N_f} \tag{4}$$

$$\mathbf{w}^*_{opt.} = d^{-1}_{N_f-1}\mathbf{e}^*_{N_f}\mathbf{L}^{-1}\mathbf{H}^*\mathbf{R}^{-1}_{nn} \ , \tag{5}$$

where $\mathbf{I}_{N_f+\nu}$ is the identity matrix of size $N_f+\nu$, $(.)^t$ denotes the transpose, $\mathbf{e}_{N_f}$ is the N_f^{th} unit vector, and d_{N_f-1} is the N_f^{th} diagonal element of $\mathbf{D}$. The minimum mean square error is equal to

$$MSE_{MMSE-DFE} = d^{-1}_{N_f-1} \ ,$$

therefore, the decision–point SNR of the FIR MMSE–DFE is given by

$$SNR_{MMSE-DFE} \stackrel{def}{=} \frac{S_x}{MSE_{MMSE-DFE}} = S_x d_{N_f-1} \ . \tag{6}$$

Now, in the presence of CNEE, Equations (3)-(5) are modified to

$$\mathbf{R}^e \stackrel{def}{=} \frac{1}{S_x^e}\mathbf{I}_{N_f+\nu^e} + \mathbf{H}^{*e}(\mathbf{R}^e_{nn})^{-1}\mathbf{H}^e \stackrel{def}{=} \mathbf{L}^e\mathbf{D}^e\mathbf{L}^{*e} \tag{7}$$

$$\tilde{\mathbf{b}}^e = \mathbf{L}^e\mathbf{e}_{N_f} \tag{8}$$

$$\mathbf{w}^{*e} = (d^e_{N_f-1})^{-1}\mathbf{e}^*_{N_f}(\mathbf{L}^e)^{-1}\mathbf{H}^{*e}(\mathbf{R}^e_{nn})^{-1} \ . \tag{9}$$

The decision–point SNR of the mismatched FIR MMSE–DFE is given by the ratio of the mismatched input energy S_x^e to the variance of the mismatched error sequence, i.e.,

$$SNR^e_{MMSE-DFE} \stackrel{def}{=} \frac{S^e_x}{MSE^e_{MMSE-DFE}} \ , \tag{10}$$

where,

[2] Assuming that the optimum decision delay is equal to (N_f-1). This assumption can be shown to hold for most practical channel and noise scenarios, especially as the feedforward filter becomes long enough [4, 5].

$$MSE^e_{MMSE-DFE} \stackrel{def}{=} \mathrm{E}[(\tilde{\mathbf{b}}^{*e}\mathbf{x}_{k+N_f-1:k-\nu^e} - \mathbf{w}^{*e}\mathbf{y}_{k+N_f-1:k})(\tilde{\mathbf{b}}^{*e}\mathbf{x}_{k+N_f-1:k-\nu^e} - \mathbf{w}^{*e}\mathbf{y}_{k+N_f-1:k})^*]$$
$$= S_x\tilde{\mathbf{b}}^{*e}\tilde{\mathbf{b}}^e - \tilde{\mathbf{b}}^{*e}\bar{\mathbf{R}}_{xy}\mathbf{w}^e - \mathbf{w}^{*e}\bar{\mathbf{R}}_{yx}\tilde{\mathbf{b}}^e + \mathbf{w}^{*e}\mathbf{R}_{yy}\mathbf{w}^e \ . \qquad (11)$$

The cross–correlation matrix $\bar{\mathbf{R}}_{xy}$ is defined as follows

$$\bar{\mathbf{R}}_{xy} \stackrel{def}{=} \begin{cases} \begin{bmatrix} \mathbf{I}_{N_f+\nu^e} & \mathbf{0}_{(N_f+\nu^e)\times(\nu-\nu^e)} \end{bmatrix} \mathbf{R}_{xy} & : \nu \geq \nu^e \\ \begin{bmatrix} \mathbf{R}_{xy} \\ \mathbf{0}_{(\nu^e-\nu)\times N_f} \end{bmatrix} & : \nu^e \geq \nu \end{cases} . \qquad (12)$$

The feedforward and feedback filter coefficients are interdependent through the relation [4]

$$\mathbf{w}^{*e} = \tilde{\mathbf{b}}^{*e}\mathbf{R}^e_{xy}(\mathbf{R}^e_{yy})^{-1} \ , \qquad (13)$$

where $\mathbf{R}^e_{xy} = S^e_x\mathbf{H}^{*e}$ and $\mathbf{R}^e_{yy} = S^e_x\mathbf{H}^e\mathbf{H}^{*e} + \mathbf{R}^e_{nn}$. Therefore, (11) becomes

$$MSE^e_{MMSE-DFE} = \tilde{\mathbf{b}}^{*e}(S_x\mathbf{I}_{N_f+\nu^e} - \bar{\mathbf{R}}_{xy}(\mathbf{R}^e_{yy})^{-1}\mathbf{R}^e_{yx} - \mathbf{R}^e_{xy}(\mathbf{R}^e_{yy})^{-1}\bar{\mathbf{R}}_{yx} + \mathbf{R}^e_{xy}(\mathbf{R}^e_{yy})^{-1}\mathbf{R}_{yy}(\mathbf{R}^e_{yy})^{-1}\mathbf{R}^e_{yx})\tilde{\mathbf{b}}^e$$
$$\stackrel{def}{=} \tilde{\mathbf{b}}^{*e}(\mathbf{R}^{\perp e}_{x/y})\tilde{\mathbf{b}}^e \ . \qquad (14)$$

Note that in the absence of CNEE, $\mathbf{R}^{\perp e}_{x/y}$ becomes equal to $S_x\mathbf{I}_{N_f+\nu} - \mathbf{R}_{xy}\mathbf{R}^{-1}_{yy}\mathbf{R}_{yx} \stackrel{def}{=} \mathbf{R}^{\perp}_{x/y} = \mathbf{R}^{-1}$.

II-B. The Mismatched FIR AMMSE-DFE

In some situations, the feedforward filter of the MMSE–DFE is implemented adaptively while the feedback filter remains fixed at its settings that were computed based on mismatched channel and noise estimates [14]. Examples include Tomlinson–Harashima precoding where the feedback filter is moved to the transmitter end or in partial response equalization where the adaptive feedforward filter equalizes the channel response to a *short* pre–determined response in order to reduce the complexity of maximum likelihood receivers [12, 5].

As in the non–adaptive MMSE–DFE, the feedback filter settings in this case are computed from (7) and (8). After convergence, the optimal feedforward filter settings are given by

$$\mathbf{w}^{*e} = \tilde{\mathbf{b}}^{*e}\bar{\mathbf{R}}_{xy}\mathbf{R}^{-1}_{yy} \ . \qquad (15)$$

Using (11) and (15), the variance of the error sequence of the mismatched AMMSE–DFE is

$$MSE^e_{AMMSE-DFE} = \tilde{\mathbf{b}}^{*e}(S_x\mathbf{I}_{N_f+\nu^e} - \bar{\mathbf{R}}_{xy}\mathbf{R}^{-1}_{yy}\bar{\mathbf{R}}_{yx})\tilde{\mathbf{b}}^e$$
$$= \begin{cases} \mathbf{e}^*_{N_f}\mathbf{L}^{*e}\begin{bmatrix} \mathbf{I}_{N_f+\nu^e} & \mathbf{0}_{(N_f+\nu^e)\times(\nu-\nu^e)} \end{bmatrix}\mathbf{L}^{-*}\mathbf{D}^{-1}\mathbf{L}^{-1}\begin{bmatrix} \mathbf{I}_{N_f+\nu^e} \\ \mathbf{0}_{(\nu-\nu^e)\times(N_f+\nu^e)} \end{bmatrix}\mathbf{L}^e\mathbf{e}_{N_f} & : \nu \geq \nu^e \\ \mathbf{e}^*_{N_f}\mathbf{L}^{*e}\begin{bmatrix} \mathbf{L}^{-*}\mathbf{D}^{-1}\mathbf{L}^{-1} & \mathbf{0}_{(N_f+\nu)\times(\nu^e-\nu)} \\ \mathbf{0}_{(\nu^e-\nu)\times(N_f+\nu)} & \mathbf{0}_{(\nu^e-\nu)\times(\nu^e-\nu)} \end{bmatrix}\mathbf{L}^e\mathbf{e}_{N_f} & : \nu^e \geq \nu \end{cases} .$$

In the absence of CNEE (i.e., $\mathbf{L}^e = \mathbf{L}$ and $\nu^e = \nu$), this expression reduces to $d_{N_f-1}^{-1} \overset{def}{=} MSE_{MMSE-DFE}$, as expected. The decision–point SNR of the mismatched adaptive MMSE–DFE is given by

$$SNR^e_{AMMSE-DFE} \overset{def}{=} \frac{S_x^e}{MSE^e_{AMMSE-DFE}} . \tag{16}$$

The following inequalities always hold

$$MSE^e_{MMSE-DFE} \geq MSE^e_{AMMSE-DFE} \geq MSE_{MMSE-DFE} .$$

II-C. The Mismatched FIR MMSE-LE

The optimum settings of a length–N_f MMSE–LE are determined from [4]

$$\begin{aligned} \mathbf{w}^*_{MMSE-LE} &= \mathbf{R}_{xy,LE}\mathbf{R}_{yy}^{-1} \\ &\overset{def}{=} \mathbf{e}^*_{\Delta+1}\mathbf{R}_{xy}\mathbf{R}_{yy}^{-1} \\ &= \mathbf{e}^*_{\Delta+1}\mathbf{H}^*(\mathbf{H}\mathbf{H}^* + \frac{\mathbf{R}_{nn}}{S_x})^{-1} . \end{aligned} \tag{17}$$

The delay parameter Δ is chosen to maximize the decision-point SNR given by [4]

$$\begin{aligned} SNR_{MMSE-LE} &\overset{def}{=} \frac{S_x}{MSE_{MMSE-LE}} \\ &= \frac{S_x}{\mathbf{R}^{\perp}_{x/y}(\Delta+1, \Delta+1)} . \end{aligned} \tag{18}$$

Under mismatch conditions, a suboptimum value of the delay (Δ^e) is used (as it will be verified through the simulations of Section III) and the mismatched MMSE–LE settings are calculated from

$$\begin{aligned} \mathbf{w}^{*e}_{MMSE-LE} &= \mathbf{R}^e_{xy,LE}(\mathbf{R}^e_{yy})^{-1} \\ &= \mathbf{e}^*_{\Delta^e+1}\mathbf{R}^e_{xy}(\mathbf{R}^e_{yy})^{-1} \\ &= \mathbf{e}^*_{\Delta^e+1}\mathbf{H}^{*e}(\mathbf{H}\mathbf{H}^{*e} + \frac{\mathbf{R}^e_{nn}}{S^e_x})^{-1} . \end{aligned} \tag{19}$$

It can be shown that the decision–point SNR of the mismatched MMSE–LE is given by

$$SNR^e_{MMSE-LE} \overset{def}{=} \frac{S_x^e}{MSE^e_{MMSE-LE}} , \tag{20}$$

where,

$$MSE^e_{MMSE-LE} = S_x - \mathbf{R}_{xy,LE}\mathbf{w}^e_{MMSE-LE} - \mathbf{w}^{*e}_{MMSE-LE}\mathbf{R}_{yx,LE} + \mathbf{w}^{*e}\mathbf{R}_{yy}\mathbf{w}^e \tag{21}$$

$$\begin{aligned} &= S_x - \mathbf{e}^*_{\Delta^e+1}(\bar{\mathbf{R}}_{xy}(\mathbf{R}^e_{yy})^{-1}\mathbf{R}^e_{yx} - \mathbf{R}^e_{xy}(\mathbf{R}^e_{yy})^{-1}\bar{\mathbf{R}}_{yx} + \mathbf{R}^e_{xy}(\mathbf{R}^e_{yy})^{-1}\mathbf{R}_{yy}(\mathbf{R}^e_{yy})^{-1}\mathbf{R}^e_{yx})\mathbf{e}_{\Delta^e+1} \\ &\overset{def}{=} \mathbf{R}^{\perp e}_{x/y}(\Delta^e+1, \Delta^e+1) . \end{aligned} \tag{22}$$

The last line follows from (14) and the fact that $\tilde{\mathbf{b}}^e = \mathbf{e}_{\Delta^e+1}$ (i.e., no feedback filter). Again, Δ^e is chosen to minimize $MSE^e_{MMSE-LE}$. This minimum value is seen from (22) to be equal to the smallest diagonal element of the matrix $\mathbf{R}^{\perp e}_{x/y}$.

An alternative expression for $MSE^e_{MMSE-LE}$ was given in [10], namely

$$\begin{aligned} MSE^e_{MMSE-LE} &= MSE_{MMSE-LE} + (\mathbf{w}^e_{MMSE-LE} - \mathbf{w}_{MMSE-LE})^* \mathbf{R}_{yy} (\mathbf{w}^e_{MMSE-LE} - \mathbf{w}_{MMSE-LE}) \\ &= S_x - \mathbf{R}_{xy,LE} \mathbf{R}_{yy}^{-1} \mathbf{R}_{yx,LE} \\ &+ (\mathbf{w}^e_{MMSE-LE} - \mathbf{w}_{MMSE-LE})^* \mathbf{R}_{yy} (\mathbf{w}^e_{MMSE-LE} - \mathbf{w}_{MMSE-LE}) \ . \end{aligned} \tag{23}$$

This equation shows explicitly the increase in mean square error (MSE) due to CNEE by expressing it as the sum of the ideal MSE and a positive term. Next, we show that (21) and (23) are equivalent.

Starting with (23) and using (17) and (19), we have

$$\begin{aligned} MSE^e_{MMSE-LE} &= S_x - \mathbf{R}_{xy,LE} \mathbf{R}_{yy}^{-1} \mathbf{R}_{yx,LE} \\ &+ (\mathbf{R}^e_{xy,LE} (\mathbf{R}^e_{yy})^{-1} - \mathbf{R}_{xy,LE} \mathbf{R}_{yy}^{-1}) \mathbf{R}_{yy} ((\mathbf{R}^e_{yy})^{-1} \mathbf{R}^e_{yx,LE} - \mathbf{R}_{yy}^{-1} \mathbf{R}_{yx,LE}) \\ &= S_x - \mathbf{R}_{xy,LE} (\mathbf{R}^e_{yy})^{-1} \mathbf{R}^e_{yx,LE} - \mathbf{R}^e_{xy,LE} (\mathbf{R}^e_{yy})^{-1} \mathbf{R}_{yx,LE} \\ &+ \mathbf{R}^e_{xy,LE} (\mathbf{R}^e_{yy})^{-1} \mathbf{R}_{yy} (\mathbf{R}^e_{yy})^{-1} \mathbf{R}^e_{yx,LE} \ , \end{aligned}$$

which is identical to (21).

A similar approach can be followed for the MMSE–DFE to derive a relation between $MSE^e_{MMSE-DFE}$ and $MSE_{MMSE-DFE}$. More specifically, by embedding the feedforward and feedback filter coefficients in a single vector, (2) can be written as follows

$$e_k = \hat{x}_k - \mathbf{v}^* \mathbf{u} \ ,$$

where,

$$\begin{aligned} \mathbf{v}^* &\stackrel{def}{=} \begin{bmatrix} w_0^* & \cdots & w_{N_f-1}^* & -b_1^* & \cdots & -b_\nu^* \end{bmatrix} \\ \mathbf{u} &\stackrel{ef}{=} \begin{bmatrix} y_{k+N_f-1} & \cdots & y_k & x_{k-1} & \cdots & x_{k-\nu} \end{bmatrix}^t \stackrel{def}{=} \begin{bmatrix} \mathbf{y} & \bar{\mathbf{x}} \end{bmatrix} \ . \end{aligned}$$

Then, in the presence of channel and noise mismatch, it can be shown that

$$MSE^e_{MMSE-DFE} = MSE_{MMSE-DFE} + (\mathbf{v}^e - \mathbf{v})^* \mathbf{R}_{uu} (\mathbf{v}^e - \mathbf{v}) \ ,$$

where,

$$\mathbf{R}_{uu} \stackrel{def}{=} \begin{bmatrix} \mathbf{R}_{yy} & \mathbf{R}_{y\bar{x}} \\ \mathbf{R}_{\bar{x}y} & \mathbf{R}_{\bar{x}\bar{x}} \end{bmatrix} = \begin{bmatrix} S_x \mathbf{H}\mathbf{H}^* + \mathbf{R}_{nn} & S_x \mathbf{H} \begin{bmatrix} \mathbf{0}_{N_f \times \nu} \\ \mathbf{I}_\nu \end{bmatrix} \\ S_x \begin{bmatrix} \mathbf{0}_{\nu \times N_f} & \mathbf{I}_\nu \end{bmatrix} \mathbf{H}^* & S_x \mathbf{I}_\nu \end{bmatrix} \ .$$

II-D. Mismatch due to Pole-Zero Approximations

In [6], we derived a computationally–efficient algorithm that approximates the FIR feedforward and feedback filters of the MMSE–DFE, in applications where these FIR filters are increased in length to achieve satisfactory performance, by pole–zero filters with much fewer coefficients. The derived pole–zero approximations were shown to be of high quality (as measured by the normalized norm tap error between the impulse responses of the original FIR filter and its pole–zero approximation) and resulted in significant savings in implementation cost. However, the degradation in the decision–point SNR of the MMSE–DFE due to the (small but nonzero) approximation errors was not examined in [6]. This effect is investigated next. In the remainder of this section, we shall assume that the channel and noise estimates are perfect and the only errors are due to the pole–zero modeling process.

For the original FIR feedforward and feedback filters, the decision–point SNR is computed using Equations (4)-(6). When the pole–zero models $b(D) \stackrel{def}{=} \frac{n^b(D)}{a^b(D)}$ and $w^*(D^{-1}) \stackrel{def}{=} \frac{n^{*w}(D^{-1})}{a^{*w}(D^{-1})}$ for the feedback and feedforward filters, respectively, are implemented, the decision–point SNR is calculated using (36) and (37) of Section IV-C with $b^e(D)$ replaced by $\frac{n^b(D)}{a^b(D)}$ and $w^{*e}(D^{-1})$ replaced by $\frac{n^{*w}(D^{-1})}{a^{*w}(D^{-1})}$.

Another situation of mismatch due to pole–zero approximation errors arises when the MMSE–DFE filters are calculated based on a pole–zero model of the channel rather than the original long FIR channel model. It is well–known (see e.g. [11]) that the optimum settings of the infinite–length MMSE–DFE can be computed from the spectral factorization

$$\frac{1}{SNR} + h(D)h^*(D^{-1}) \stackrel{def}{=} \gamma_0^2 g(D) g^*(D^{-1})\,, \tag{24}$$

as follows

$$\begin{aligned} b(D) &= g(D) && (25)\\ w^*(D^{-1}) &= \frac{b(D)R_{xy}(D)}{R_{yy}(D)} \\ &= \frac{1}{\gamma_0^2}\frac{h^*(D^{-1})}{g^*(D^{-1})}\,, && (26) \end{aligned}$$

and the decision–point SNR is equal to $\gamma_0^2 SNR$.

On highly dispersive channels (i.e., ν is large), significant computational savings can be achieved by computing the MMSE–DFE settings based on a reduced–parameter pole–zero model of the channel $h(D) \approx \frac{n^h(D)}{a^h(D)}$. In this case, it can be shown [6] that the MMSE–DFE settings are computed from

$$\begin{aligned} \frac{1}{SNR}a^h(D)a^{*h}(D^{-1}) + n^h(D)n^{*h}(D^{-1}) &\stackrel{def}{=} \gamma_0^2 r(D) r^*(D^{-1}) \\ b(D) &\approx \frac{r(D)}{a^h(D)} \\ w^*(D^{-1}) &\approx \frac{1}{\gamma_0^2}\frac{n^{*h}(D^{-1})}{r^*(D^{-1})}\,. \end{aligned}$$

The auto–correlation function of the error sequence in this case is identical to that of Equation (37) in Section IV-C *except* that $b^e(D) = \frac{r(D)}{a^h(D)}$, and the correlation functions $R^e_{xy}(D)$, $R^e_{yx}(D)$, and $R^e_{yy}(D)$ are based on the channel pole–zero model $h(D) \approx \frac{n^h(D)}{a^h(D)}$.

III. Simulation Results

In this section, we shall present computer simulation results that quantify the effect of CNEE on performance of the FIR MMSE–DFE, FIR AMMSE–DFE, and FIR MMSE–LE.

The simulation parameters are typical of the high–bit–rate digital subscriber loop (HDSL) environment [1]. More specifically, the channel studied is a 9 kft 26 American Wire Gauge (AWG) loop [1], the target bit rate is 800 kbps, and the input signal constellation is a 16–point quadrature amplitude modulation (QAM) constellation. The input power level is 17 dBm equally–distributed over the transmission bandwidth. The noise consists of a white component with a one–sided power spectral density (psd) of -110 dBm/Hz, and a colored component due to near–end crosstalk (NEXT) where the standard $K_{NEXT} f^{\frac{3}{2}}$ model is assumed with $K_{NEXT} = 10^{-13}$ [8]. The number of feedforward equalizer taps is equal to 64 and the number of feedback taps is equal to the channel memory, after truncating the latter using a 99.9% energy criterion.

Channel mismatch could manifest itself in several forms including time–domain errors whether they are impulsive, multiplicative, or additive errors affecting the CIR coefficients or errors in determining the CIR length. The channel errors could also be wideband or concentrated in a certain range of the channel frequency response, where errors are most likely to occur. Similarly, noise mismatch could manifest itself in the form of a misestimated variance for white noise [10] or more generally in the form of a misestimated noise correlation profile for colored noise. In all cases, mismatch includes both over– or under– estimating the true value. For the purposes of this paper, the effects of channel mismatch are modeled by *assuming a fixed percentage of over- or under- estimation of the channel frequency response in the frequency range* $0 - 50$ *kHz*. In particular, the *channel matching percentage* is defined as the *ratio of the misestimated channel frequency response to the true channel frequency response, in the range* $0 - 50$ *kHz, multiplied by* 100. This particular model was chosen for illustration purposes and because channel estimation errors for digital subscriber lines are most likely to occur in this frequency range (see e.g. [14, 6]). The effects of noise mismatch were modeled by *assuming the noise to be white with a fixed (mismatched) psd* when it is actually colored because of the presence of crosstalk. *We emphasize that other channel and noise mismatch models can be accommodated as well using the general expressions derived in Section II.*

III-A. Effect of Channel Mismatch

Figure 1 shows the degradation of the decision–point SNR of the FIR MMSE–LE, the FIR AMMSE–DFE, and the FIR MMSE–DFE with the channel matching percentage.

It is evident from the plot that the FIR MMSE–DFE is *very sensitive to channel mismatch.* The use of an adaptive feedforward filter in the FIR AMMSE–DFE structure reduces this sensitivity significantly. Also, the FIR MMSE–LE is seen to be more robust towards channel mismatch than the FIR MMSE–DFE. In fact, beyond a certain percentage of channel mismatch, the mismatched FIR MMSE–LE performs better than the mismatched FIR MMSE–DFE. This is due to the presence of the feedback filter of the MMSE–DFE which tends to exacerbate the effects of mismatch.

To examine the effects of the number of feedforward taps and the input power level on performance, we have plotted the variation of the decision–point SNR with these two parameters (assuming a 20% channel underestimation error or equivalently an 80% channel matching percentage) in Figures 2 and 3, respectively.

The effect of N_f on performance becomes negligible only as N_f becomes large enough (around 20 taps for the DFE and 80 taps for the LE for the assumed scenario) in which case the asymptotic sensitivity analysis of [14, 10] (see also Section IV-C) becomes more accurate. However, when complexity considerations entail the choice of a small N_f, the asymptotic analyses no longer hold and must be replaced by the finite–length analysis of Section II. It can also be seen from Figure 2 that while the decision–point SNR of the ideal FIR MMSE–DFE increases monotonically with N_f, this is no longer true in the presence of mismatch. This effect was termed the *complexity inversion phenomenon* and analyzed extensively in [10].

As expected, performance degradation due to channel mismatch becomes more significant at higher input power levels, especially for the MMSE–DFE, as shown in Figure 3. This can be attributed to the fact that at high input power levels, the effects of mismatch dominate over those of the additive noise.

III-B. Effect of Noise Mismatch

Figure 4 shows the effect of assuming the noise to be white with a mismatched psd, when it is actually correlated, on the decision–point SNR. It can be inferred from the plot that, for the particular scenario under consideration, the MMSE–DFE suffers about 2 dB loss in its decision–point SNR when the noise correlation (due to crosstalk in this case) is not taken into account. Furthermore, this loss is virtually constant unless the mismatched noise psd is very high (more than -90 dBm/Hz). On the other hand, the MMSE–LE is much more robust to noise mismatch than the MMSE–DFE. It is also worth mentioning that zero–forcing equalizers are insensitive to noise mismatch [10] because the computation of their filter settings does not take noise into account [12]. However, they could be more sensitive to channel mismatch than MMSE equalizers, especially on channels with spectral nulls.

III-C. Delay Mismatch

It is evident from (18) that optimizing the delay is an important part of maximizing the decision–point SNR of the MMSE–LE. Optimization of the delay is based on knowledge of the channel and noise characteristics [5]. Therefore, the presence of estimation errors causes the computed optimum delay to deviate from the actual optimum delay that is based on the true channel and noise characteristics. An example of that deviation is plotted versus the channel matching percentage in Figure 5.

More significant variation of the optimum delay and performance degradation due to delay mismatch occur for the case of a MMSE–DFE with a feedback filter length, denoted by N_b, less than the channel memory, as shown in Figure 6

III-D. Sensitivity to Pole-Zero Modeling

Figure 7 shows the degradation in the decision–point SNR when the 8–pole 7–zero model of the 9 kft 26 AWG loop that was derived in [6] is used to approximate its long FIR impulse response for different input power levels. Hence, the "mismatch" here is due to computing the receiver filters based on a pole–zero approximation of the true channel impulse response. Again, it is evident from the figure that the performance degradation is more pronounced for the MMSE–DFE than it is for the AMMSE–DFE or the MMSE–LE and that it increases at higher input power levels.

We found that a better alternative is to compute the MMSE–DFE filters based on the original long FIR model of the channel (using the algorithms of [3]) and then approximate them by pole–zero filters to reduce the implementation cost [6]. More specifically, using the 4–pole 4–zero model for the 64–tap feedback filter together with the 5–pole 2–zero and the 2–pole 1–zero models for the 2 components of the 96–tap feedforward filter that were given in [6], we found that the decision–point SNR decreases from 22.1 dB to 21.05 dB at an input power level of 17 dBm.

In concluding this section, we shall summarize the main factors that determine the amount of performance degradation due to mismatch. These factors include the receiver structure, the amount of mismatch, the nature of the channel (severity of intersymbol interference, presence of spectral nulls, speed of time variations, $\cdots$), the degree of noise correlation, the complexity of the receiver (number of equalizer taps), and the particular implementation of the receiver (all-zero, pole–zero, cascade, lattice, $\cdots$). In [10], the variation of the quantity $\frac{\max(|H(e^{j\Theta})|^2)}{\min(|H(e^{j\Theta})|^2)}$ with the level of channel mismatch was proposed as an indicator of the amount of performance degradation to be expected, for the case of white noise and infinite–length filters. Based on our analysis of Section II, we propose the generalization of this measure to $\frac{\lambda_{max}(\mathbf{H}^*\mathbf{R}_{nn}^{-1}\mathbf{H})}{\lambda_{min}(\mathbf{H}^*\mathbf{R}_{nn}^{-1}\mathbf{H})}$ for the case of colored noise and finite–length filters, where $\lambda_{max}(.)$ and $\lambda_{min}(.)$ denote the maximum and minimum eigenvalue, respectively.

IV. Related Issues

IV-A. Sensitivity of DMT to Mismatch

In the DMT implementation of multichannel modulation [13], the independence of the IDFT/DFT modulating/demodulating vectors from the channel and noise characteristics and the use of a flat input energy distribution [3] increase the robustness of the DMT against CNEE. However, determination of the number of usable subchannels $\bar{N}$ (or equivalently the transmission bandwidth) and the allocation of the transmitted input bits to these subchannels are *dependent* on the subchannels' SNRs.

With perfect channel and noise estimates and assuming a constant probability of symbol error across the usable subchannels, the output SNR of the DMT can be calculated as follows [14]

$$SNR_{DMT} \approx \frac{S_x}{\bar{N}}[\prod_{i=1}^{\bar{N}}(\frac{|H_i|^2}{R_{nn,i}})]^{\frac{1}{\bar{N}}} \ , \tag{27}$$

where $|H_i|^2$ and $R_{nn,i}$ are the channel gain and the noise psd at the i^{th} subchannel, respectively.

In the presence of CNEE, the input bit distribution and transmission bandwidth will be different from their values with perfect channel and noise estimates. *This mismatch causes the probability of error to vary across the subchannels.* As described in detail in [14], the output SNR of the mismatched DMT can be approximated as follows

$$SNR^e_{DMT} \approx \frac{\gamma_m}{\gamma_{eff}}\frac{(Q^{-1}(\bar{P}^e_e))^2}{3}(2^{\bar{b}^e}-1) \ , \tag{28}$$

where γ_m is the desired DMT performance margin, γ_{eff} is the applied coding gain (if any), and

$$\bar{P}^e_e = \frac{\sum_{i=1}^{\bar{N}^e} P^e_{e,i} b^e_i}{\sum_{i=1}^{\bar{N}^e} b^e_i}; \ \bar{b}^e = \frac{1}{\bar{N}^e}\sum_{i=1}^{\bar{N}^e} b^e_i \ .$$

b^e_i and $\bar{N}^e$ are the number of bits allocated to the i^{th} subchannel and the number of usable subchannels, respectively, *both based on the misestimated channel and noise characteristics.* $P^e_{e,i}$ is the probability of symbol error on the i^{th} subchannel resulting from the mismatched bit distribution and is given by

$$P^e_{e,i} = Q(\sqrt{3\frac{\gamma_{eff}}{\gamma_m}\frac{\frac{S_x}{\bar{N}^e}\frac{|H_i|^2}{R_{nn,i}}}{(2^{b^e_i}-1)}}).$$

[3] The flat energy distribution has been shown to be near optimum, as long as the transmission bandwidth is optimized.

In Figure 8, we have plotted the variation of the DMT decision–point SNR versus the input power level assuming a perfect channel estimate and under the 20% channel underestimation error conditions described in Section III. It is evident from the plot that the DMT is much less sensitive to channel estimation errors than the MMSE–DFE. Furthermore, the small performance degradation of the DMT due to channel mismatch remains almost constant for a wide range of input power levels unlike the MMSE–DFE where it becomes more pronounced at higher input power levels.

IV-B. Reducing the Sensitivity to Mismatch

Several measures can be undertaken to reduce performance degradation due to CNEE including

1. The use of more *robust* receivers, such as the DMT (see Section IV-A), the recursive least squares estimation (RLSE) receiver of [10], or the MMSE–LE on channels with mild intersymbol interference.
2. Improving the quality and computational efficiency of the channel and noise estimates obtained during training (see e.g. [9]).
3. The use of adaptive transmitters and receivers that continuously track time variations in the channel and noise estimates that were obtained during training [12, 7]. The frequency of adaptation represents a trade–off between complexity and performance.
4. For channel–estimate–based receivers [15], continuous adaptation of the channel and noise estimates in the case of time variations in the environment and devising fast algorithms for computing the receiver filter settings from channel and noise estimates (such as the DFE algorithms of [3]) are essential to prevent significant performance loss due to mismatch.
5. Using implementations that are less sensitive to round–off and finite–precision effects.

IV-C. Asymptotic Analysis

In this section, the degradation in the decision–point SNR due to mismatch as the number of feedforward taps N_f becomes infinite is examined. In this case, the input–output cross–correlation and the output auto–correlation functions are given by $R_{xy}(D) = S_x h^*(D^{-1})$ and $R_{yy}(D) = S_x h(D) h^*(D^{-1}) + R_{nn}(D)$, respectively. Their mismatched counterparts $R^e_{xy}(D)$ and $R^e_{yy}(D)$ are obtained by replacing S_x with S^e_x, $h(D)$ with $h^e(D)$, and $R_{nn}(D)$ with $R^e_{nn}(D)$.

- **The Infinite-Length MMSE-LE**

The error sequence of the mismatched infinite–length MMSE–LE is given by

$$e(D) = x(D) - w^e(D)y(D) \ , \tag{29}$$

where the mismatched equalizer settings are determined from $w^e(D) = \frac{R^e_{xy}(D)}{R^e_{yy}(D)}$.

Therefore, the mean square error is given by

$$MSE^e_{MMSE-LE} = \frac{1}{2\pi}\int_{-\pi}^{\pi} R^e_{ee,MMSE-LE}(e^{j\Theta})d\Theta \ , \tag{30}$$

where,

$$R^e_{ee,MMSE-LE}(D) = S_x - \frac{R_{xy}(D)R^e_{yx}(D)}{R^e_{yy}(D)} - \frac{R^e_{xy}(D)R_{yx}(D)}{R^e_{yy}(D)} + \frac{R^e_{xy}(D)R_{yy}(D)R^e_{yx}(D)}{(R^e_{yy}(D))^2} \ . \tag{31}$$

This expression reduces to the well–known relation (see e.g. [12]) $R_{ee,MMSE-LE}(D) = \frac{R_{xx}(D)R_{nn}(D)}{R_{yy}(D)}$, which holds for error–free channel and noise estimates.

In [10], the following alternative expression for $R^e_{ee,MMSE-LE}(D)$ was derived using a different approach from ours [4]

$$\begin{aligned} R^e_{ee,MMSE-LE}(D) &= \frac{R_{nn}(D)}{h(D)h^*(D^{-1}) + R_{nn}(D)} \\ &+ \frac{|(h(D)h^*(D^{-1}) + R_{nn}(D))h^e(D) - (h^e(D)h^{*e}(D^{-1}) + R^e_{nn}(D))h(D)|^2}{(h^e(D)h^{*e}(D^{-1}) + R^e_{nn}(D))^2(h(D)h^*(D^{-1}) + R_{nn})} \ . \end{aligned} \tag{32}$$

Next, we show that (32) is identical to (31). Starting with (32),

$$\begin{aligned} R^e_{ee,MMSE-LE}(D) &= \frac{R_{nn}(D)}{R_{yy}(D)} + \frac{|R_{yy}(D)h^e(D) - R^e_{yy}(D)h(D)|^2}{(R^e_{yy}(D))^2 R_{yy}(D)} \\ &= \frac{R_{nn}(D)}{R_{yy}(D)} + \frac{R_{yy}(D)h^e(D)h^{*e}(D^{-1})}{(R^e_{yy}(D))^2} - \frac{h^e(D)h^*(D^{-1})}{R^e_{yy}(D)} - \frac{h(D)h^{*e}(D^{-1})}{R^e_{yy}(D)} \\ &+ \frac{h(D)h^*(D^{-1})}{R_{yy}(D)} \\ &= 1 + \frac{R_{yy}(D)R^e_{xy}(D)R^e_{yx}(D)}{(R^e_{yy}(D))^2} - \frac{R^e_{xy}(D)R_{yx}(D)}{R^e_{yy}(D)} - \frac{R_{xy}(D)R^e_{yx}(D)}{R^e_{yy}(D)} \ , \end{aligned}$$

which is the same as (31).

- **The Infinite–Length MMSE-DFE**

[4] For simplicity and without loss of generality, S_x was assumed to be equal to 1 in [10].

As the number of feedforward taps becomes infinite, the Cholesky factorization of (7) converges to the spectral factorization

$$R^e(D) = \frac{1}{S_x^e} + \frac{h^e(D)h^{*e}(D^{-1})}{R_{nn}^e(D)} \stackrel{def}{=} (\gamma_0^e)^2 g^e(D) g^{*e}(D^{-1}) \ , \tag{33}$$

and the mismatched filter settings of the infinite–length MMSE–DFE are given by

$$\begin{aligned} b^e(D) &= g^e(D) && (34)\\ w^{*e}(D^{-1}) &= \frac{1}{(\gamma_0^e)^2}\frac{h^{*e}(D^{-1})}{g^{*e}(D^{-1})} \ . && (35)\end{aligned}$$

Therefore, the decision–point mean squared error in the presence of mismatch is

$$MSE^e_{MMSE-DFE} = \frac{1}{2\pi}\int_{-\pi}^{\pi} R^e_{ee,MMSE-DFE}(e^{j\Theta})d\Theta \ , \tag{36}$$

where,

$$\begin{aligned} R^e_{ee,MMSE-DFE}(D) &\stackrel{def}{=} \mathrm{E}[(b^e(D)x(D) - w^{*e}(D^{-1})y(D))(b^e(D)x(D) - w^{*e}(D^{-1})y(D))^*] \\ &= S_x b^e(D)b^{*e}(D^{-1}) - b^{*e}(D^{-1})R_{yx}(D)w^{*e}(D^{-1}) - b^e(D)R_{xy}(D)w^e(D) \\ &+ w^{*e}(D^{-1})R_{yy}(D)w^e(D) \\ &= b^e(D)(S_x - \frac{R^e_{xy}(D)R_{yx}(D)}{R^e_{yy}(D)} - \frac{R_{xy}(D)R^e_{yx}(D)}{R^e_{yy}(D)} \\ &+ \frac{R^e_{xy}(D)R_{yy}(D)R^e_{yx}(D)}{(R^e_{yy}(D))^2})b^{*e}(D^{-1}) && (37)\\ &= b^e(D)R^e_{ee,MMSE-LE}(D)b^{*e}(D^{-1}) \ . \end{aligned}$$

Now, if we define the spectral factorization

$$R^e_{ee,MMSE-LE}(D) \stackrel{def}{=} \eta_0^2 m(D)m^*(D^{-1}) \ , \tag{38}$$

then, by combining (36), (37), and (38), we get

$$\begin{aligned} MSE^e_{\infty MMSE-DFE} &= \frac{1}{2\pi}\int_{-\pi}^{\pi} \eta_0^2 b^e(e^{j\Theta})m(e^{j\Theta})b^{*e}(e^{-j\Theta})m^*(e^{-j\Theta})d\Theta \\ &= \eta_0^2 = e^{\frac{1}{2\pi}\int_{-\pi}^{\pi}\ln(R^e_{ee,MMSE-LE}(e^{j\Theta}))d\Theta} \ . \end{aligned}$$

The last expression is identical to the one given in [10]. It is also worth mentioning that with perfect channel and noise estimates, the error sequence becomes *white*.

- **The Adaptive Infinite-Length MMSE-DFE**

  In this case, the feedback filter is still given by (34), while the feedforward filter (after convergence) is given by

$$w^{*e}(D^{-1}) = \frac{b^e(D)R_{xy}(D)}{R_{yy}(D)} \; . \tag{39}$$

  The auto–correlation function of the error sequence in this case is given by

$$\begin{aligned} R^e_{ee,AMMSE-DFE}(D) &= \frac{S_x b^e(D) R_{nn}(D) b^{*e}(D^{-1})}{R_{yy}(D)} \\ &= \frac{1}{(\gamma_0^e)^2} \frac{\left(\frac{1}{S_x^e} + \frac{h^e(D)h^{*e}(D^{-1})}{R^e_{nn}(D)}\right)}{\left(\frac{1}{S_x} + \frac{h(D)h^{*}(D^{-1})}{R_{nn}(D)}\right)} \; . \end{aligned}$$

  Therefore,

$$MSE^e_{\infty AMMSE-DFE} = e^{\frac{1}{2\pi}\int_{-\pi}^{\pi}\ln\left(\frac{1}{S_x^e}+\frac{h^e(e^{j\Theta})h^{*e}(e^{-j\Theta})}{R^e_{nn}(e^{j\Theta})}\right)d\Theta} \frac{1}{2\pi}\int_{-\pi}^{\pi} \frac{\left(\frac{1}{S_x^e} + \frac{h^e(e^{j\Theta})h^{*e}(e^{-j\Theta})}{R^e_{nn}(e^{j\Theta})}\right)}{\left(\frac{1}{S_x} + \frac{h(e^{j\Theta})h^{*}(e^{-j\Theta})}{R_{nn}(e^{j\Theta})}\right)} d\Theta \; .$$

  Again, the error sequence becomes white in the absence of channel and noise estimation errors.

V. Conclusions

We presented a detailed sensitivity analysis for the finite–length MMSE–DFE, AMMSE-DFE, MMSE–LE, and DMT under arbitrary channel and noise mismatch conditions. The MMSE–DFE was shown to be the most sensitive towards channel and noise mismatch among the four receiver structures because of the action of its feedback filter, especially at higher input power levels.

The asymptotic forms of the derived finite–length sensitivity expressions, as the filters' lengths become infinite, were also given. Finally, several methods for reducing performance degradation due to channel and noise mismatch were described.

References

[1] IEEE Journal on Selected Areas in Communications, August 1991. Special Issue on High-Speed Digital Subscriber Lines.

[2] N. Al-Dhahir and J.M.Cioffi. "Bandwidth Optimization for Combined Equalization and Coding Transceivers with Emphasis on the MMSE-DFE". In *IEEE Milcom*, volume 2, pages 471–475, Bedford, MA, October 1993.

[3] N. Al-Dhahir and J.M.Cioffi. "Fast Computation of Channel-Estimate Based Equalizers in Packet Data Transmission". *IEEE Transactions on Signal Processing*, 43(11):2462–2473, November 1995.

[4] N. Al-Dhahir and J.M.Cioffi. "MMSE Decision Feedback Equalizers : Finite-Length Results". *IEEE Transactions on Information Theory*, 41(4):961–976, July 1995.

[5] N. Al-Dhahir and J.M.Cioffi. "Efficiently-Computed Reduced-Parameter Input-Aided MMSE Equalizers for ML Detection : A Unified Approach". *IEEE Transactions on Information Theory*, pages 903–915, May 1996.

[6] N. Al-Dhahir, A. H. Sayed, and J.M.Cioffi. "A High-Performance Cost-Effective Pole-Zero MMSE-DFE". In *Allerton Conference on Communication, Control, and Computing*, pages 1166–1175, September 1993.

[7] J. Chow, J.M.Cioffi, and J. Bingham. "Equalizer Training Algorithms for Multicarrier Modulation Systems". In *International Conference on Communications, Geneva*, pages 761–765, May 1993.

[8] J. Chow, J. Tu, and J.M.Cioffi. "A Discrete Multitone Transceiver System for HDSL Applications". *IEEE Journal on Selected Areas in Communications*, 9(6):895–908, August 1991.

[9] S. Crozier. *"Short-Block Equalization Techniques Employing Channel Estimation for Fading Time-Dispersive Channels"*. PhD thesis, Carleton University, 1989.

[10] F. Gozzo. *"Robust Sequence Estimation in the Presence of Channel Mismatch"*. PhD thesis, Rensselaer Poly. Inst., May 1992.

[11] J.M.Cioffi, G. Dudevoir, M. Eyuboglu, and G.D. Forney. "Minimum Mean-Square-Error Decision Feedback Equalization and Coding - Parts I and II". *IEEE Transactions on Communications*, October 1995.

[12] S. Qureshi. "Adaptive Equalization". *Proceedings of the IEEE*, 73(9), September 1985.

[13] A. Ruiz, J.M. Cioffi, and S. Kasturia. "Discrete Multiple Tone Modulation with Coset Coding for the Spectrally Shaped Channel". *IEEE Transactions on Communications*, 40(6):1012–1029, June 1992.

[14] J. Tu. *"Theory, Design, and Application of Multi-Channel Modulation for Digital Communications"*. PhD thesis, Stanford University, June 1991.

[15] R. Ziegler, N. Al-Dhahir, and J.M.Cioffi. "Nonrecursive Adaptive Decision-Feedback Equalization from Channel Estimates". In *Proceedings of IEEE Vehicular Technology Society* 42^{nd} *VTS Conference*, volume 2, pages 600–603, Denver, May 1992.

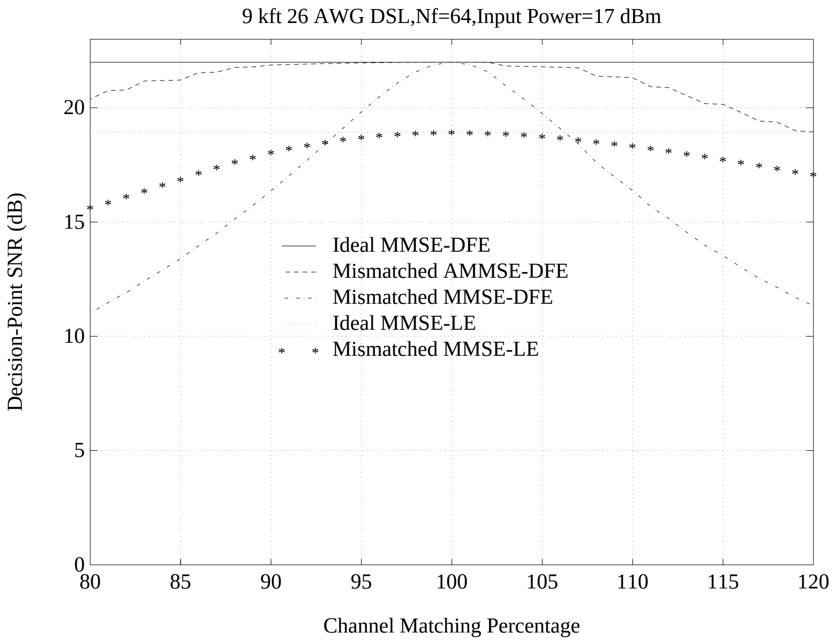

Fig. 1. Effect of channel mismatch on the decision–point SNR

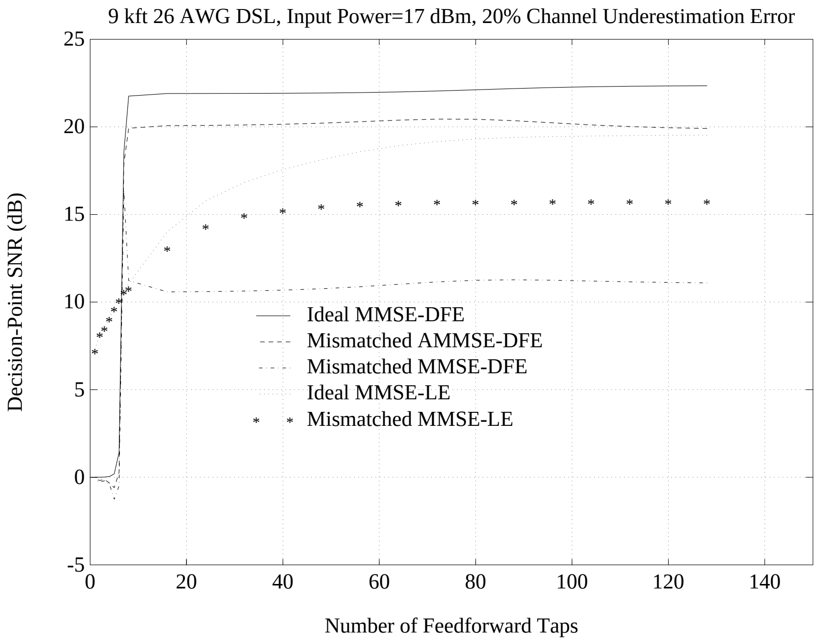

Fig. 2. Effect of channel mismatch on decision–point SNR for different numbers of feedforward taps

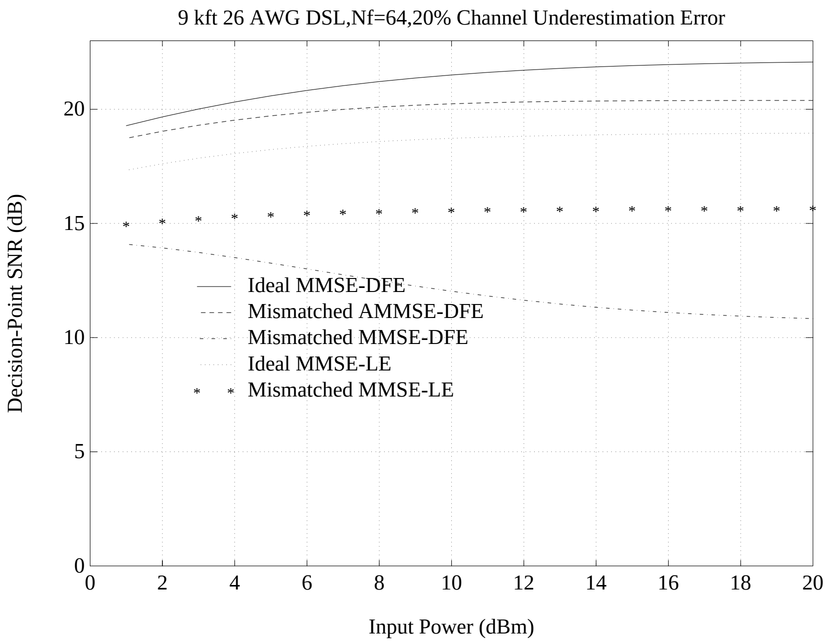

Fig. 3. Effect of channel mismatch on decision–point SNR for different input power levels

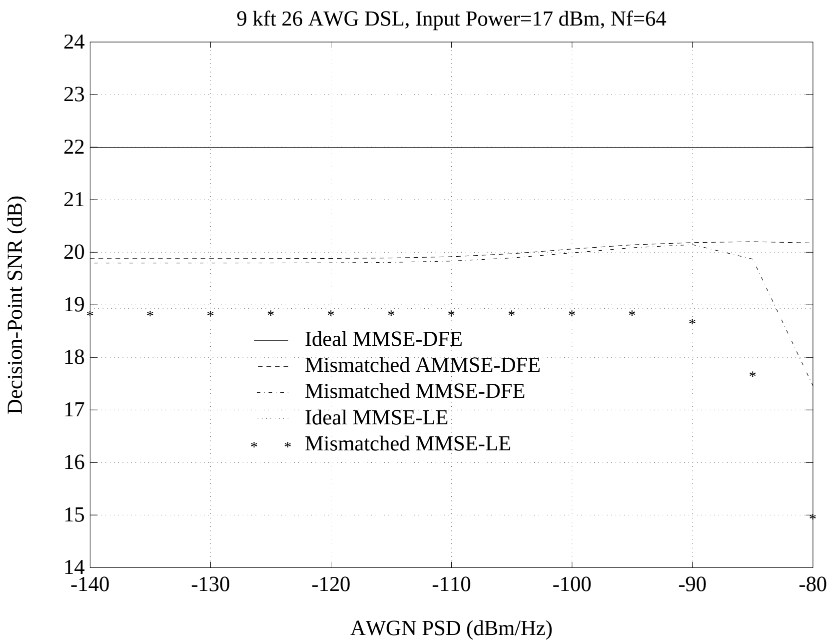

Fig. 4. Effect of noise mismatch on the decision-point SNR

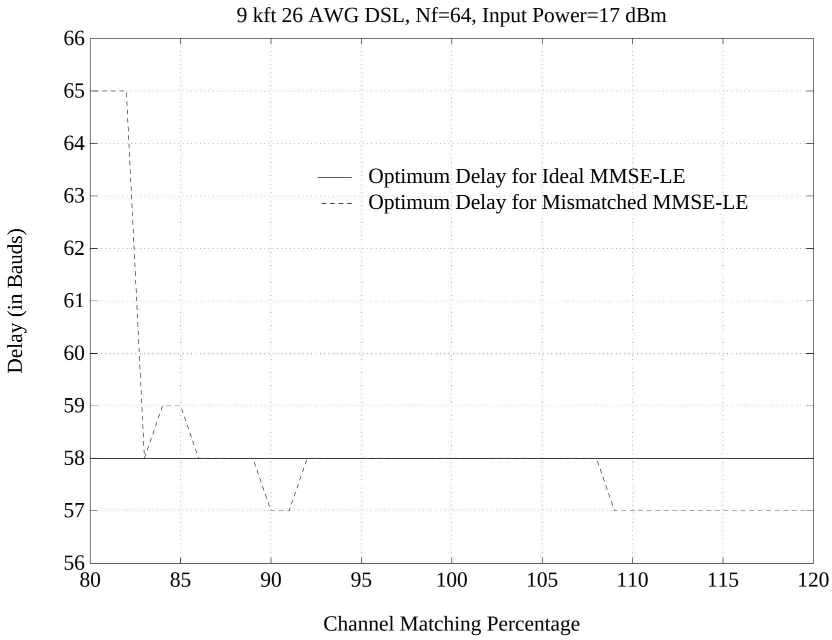

Fig. 5. Effect of channel mismatch on the optimum delay of the FIR MMSE-LE

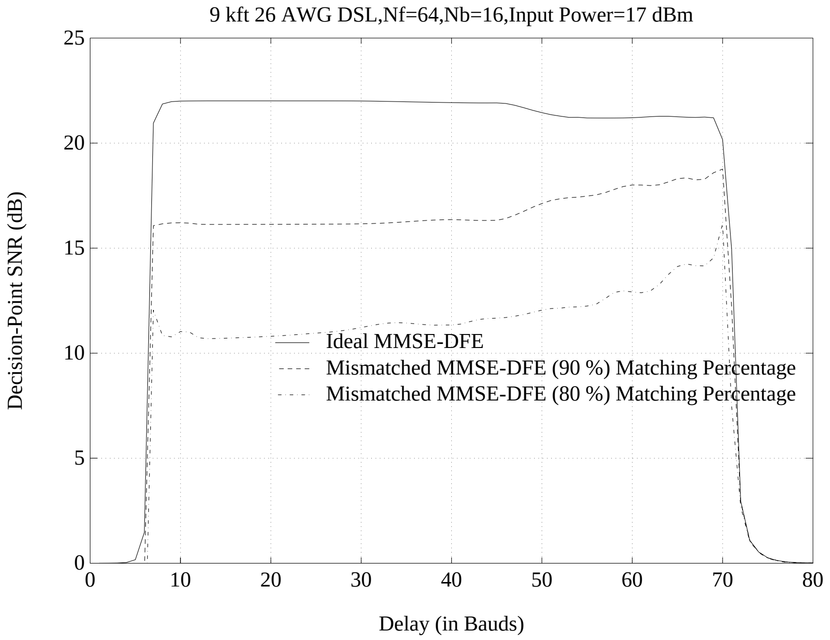

Fig. 6. Effect of channel and delay mismatch on the decision–point SNR of the FIR MMSE-DFE

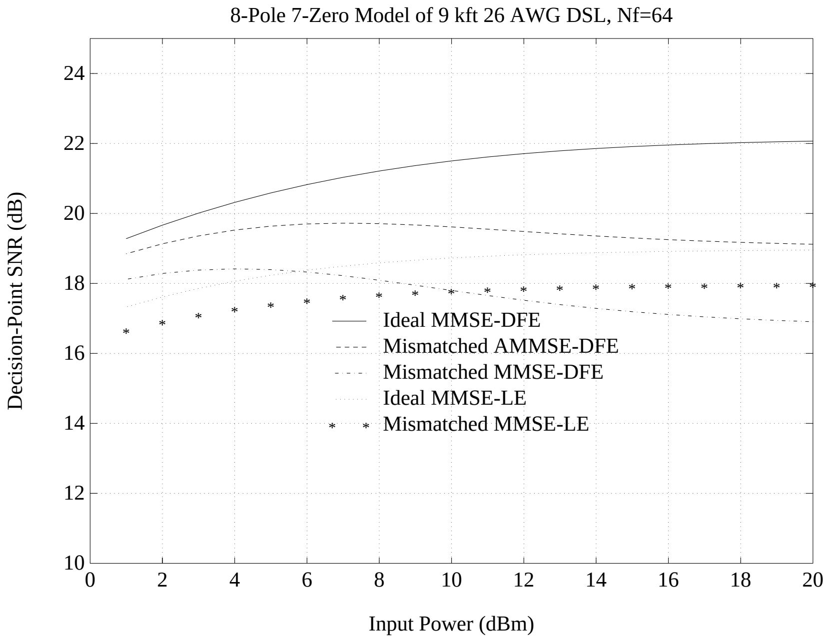

Fig. 7. Effect of pole-zero channel modeling on the decision–point SNR

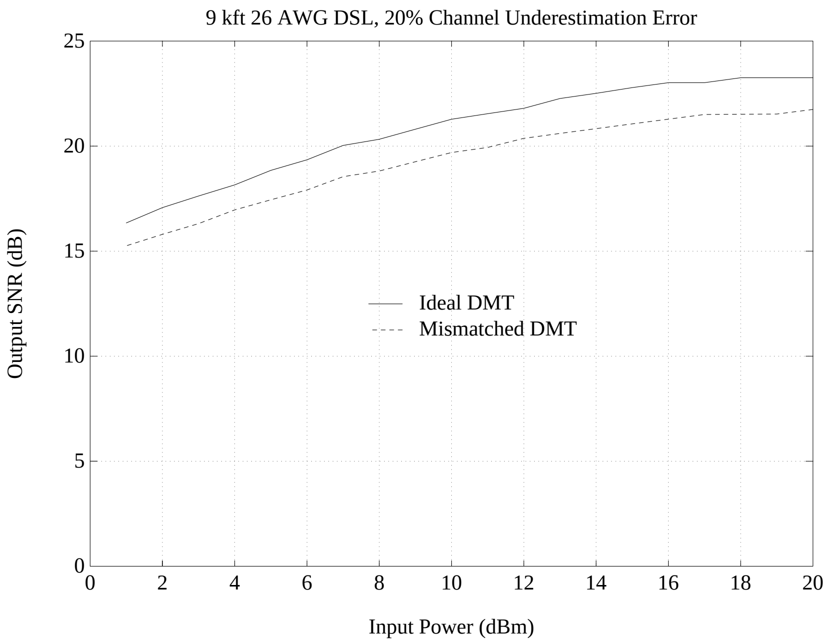

Fig. 8. Sensitivity of the DMT to channel mismatch for different input power levels

List of Figures